HHS Public Access

Author manuscript

J Med Chem. Author manuscript; available in PMC 2019 July 18.

Published in final edited form as:

J Med Chem. 2018 March 08; 61(5): 2118–2123. doi:10.1021/acs.jmedchem.8b00028.

Radiosynthesis and in Vivo Evaluation of [^{11}C]MPC-6827, the First Brain Penetrant Microtubule PET Ligand

J. S. Dileep Kumar[*,†,⊥], **Kiran Kumar Solingapuram Sai**[‡,⊥], **Jaya Prabhakaran**[†,§], **Hakeem R. Oufkir**[‡], **Gayathri Ramanathan**[‡], **Christopher T. Whitlow**[‡], **Hima Dileep**[†,§], **Akiva Mintz**[‡,‖], and **J. John Mann**[†,§]

[†]Molecular Imaging and Neuropathology Division, New York State Psychiatric Institute, 1051 Riverside Drive, New York, New York 10032, United States

[‡]Department of Radiology, Wake Forest Medical Center, Winston Salem, North Carolina 27157, United States

[§]Department of Psychiatry, Columbia University Medical Center, New York, New York 10032, United States

Abstract

Abnormalities of microtubules (MTs) are implicated in the pathogenesis of many CNS diseases. Despite the potential of an MT imaging agents, no PET ligand is currently available for in vivo imaging of MTs in the brain. We radiolabeled [^{11}C]MPC-6827, a high affinity MTA, and demonstrated its specific binding in rat and mice brain using PET imaging. Our experiments show that [^{11}C]MPC-6827 has specific binding to MT in brain, and it is the first MT-binding PET ligand.

Graphical Abstract

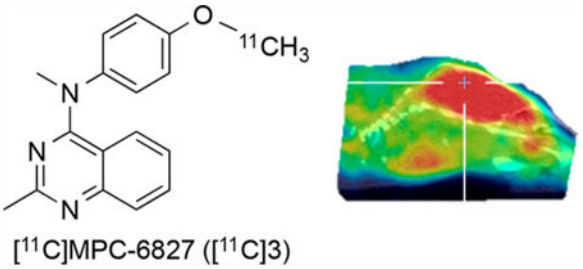

[^{11}C]MPC-6827 ([^{11}C]3)

[*]**Corresponding Author** Phone: 646-774-7522. Fax: 646-774-7521. kumardi@ nyspi.columbia.edu.

[‖]**Present Address:** For A.K.: Department of Radiology, Columbia University Medical Center, New York, New York 10032, United States.

[⊥]J.S.D.IK and K.K.S.S. contributed equally to this work.

ASSOCIATED CONTENT

Supporting Information

The Supporting Information is available free of charge on the ACS Publications website at DOI: 10.1021/acs.jmed-chem.8b00028.

Molecular formula strings of key chemicals (PDF)

Molecular formula strings of key chemicals (CSV)

The authors declare no competing financial interest.

INTRODUCTION

Microtubules (MTs) are a major component of cytoskeletal polymers and comprise repeating, noncovalently bound α- and β-tubulin heterodimers.[1,2] A major function of MT is to serve as cellular conveyer belt ferrying vesicles, granules, and organelles like mitochondria and chromosomes throughout cells. Mutations associated with MT dynamics lead to an imbalance between cell divisions, causing reduced or excessive cell proliferation that can result in cancer, birth disorders, and brain diseases.[3–5] MT-targeting agents (MTA) are among the most successful in anticancer therapy, and many MT-related drugs are in various stages of clinical development. Three classes of ligands (e.g., vinca alkaloids, paclitaxel, and derivatives and colchicine) are currently marketed for the treatment of several malignancies and other diseases.[6–8] However, these drugs have several limitations preventing their clinical applications such as high level of neurological and bone marrow toxicity, emergence of drug-resistant tumor cells due to the overproduction of multidrug resistance protein 1 (MDR1), permeability glycoprotein (P-gp), breast cancer resistance protein (BCRP), and overexpression of different tubulins or tubulin mutations. To overcome these hurdles, several new generation MTAs exhibiting promising results are in clinical trials for cancer and tauopathies.[5,8–10]

MTs in mammalian brain comprise approximately 20% of total brain protein compared with 3–4% of total protein in somatic tissues.[5] In the brain, MTs act as a quantum computer involving a complex cascade of biological processes that include mitotic division, relocation of migrating neurons, and the extension of dendritic and axonal processes. Disruption of the structural integrity of the MT network and interruption of MT function contribute to the pathophysiology of central nervous system (CNS) disorders such as Alzheimer's disease (AD).[5,11] MT loss is also reported in Parkinson's disease (PD), progressive supranuclear palsy (PSP), and corticobasal degeneration (CBD), amyotrophic lateral sclerosis (ALS), hereditary spastic paraplegia (HSP), multiple sclerosis (MS), Huntington's disease (HD), traumatic brain injury (TBI), chronic traumatic encephalopathy (CTE), and spinal cord injury (SCI).[4,5,12–18] MT loss or reduction in MT mass from axons and dendrites is also associated with normal aging and neuropsychiatric diseases.[5,18,19] MTs, specifically the βIII-tubulin isoform, are overabundant in high-grade gliomas, particularly in glioblastoma multiform (GBM).[20–22] Most older MT-binding drugs did not show benefits in the context of GBM or brain malignancies despite efficacy in non-CNS cancers. The lack of a MT binding imaging agent hampers drug development for brain diseases involving MTs. A BBB penetrating PET ligand that can quantify MTs noninvasively would permit imaging a variety of CNS disorders including brain malignancies and the conduct of target occupancy studies of potential therapeutic drugs.

[^{11}C]Paclitaxel, [^{18}F]fluoropaclitaxel, and [^{11}C]docetaxel are the successful radiotracers reported so far for MT imaging.[23] Of the three tracers, [^{18}F]fluoropaclitaxel and [^{11}C]docetaxel have been assessed in preclinical and clinical studies. Because docetaxel and paclitaxel are well-characterized substrates of efflux transporters (P-gp, MDR1, BCRP), they have little uptake brain and are not suitable for brain imaging.[23–25] [^{11}C]colchicine, another MT binding drug (IC_{50} = 3 μM), has been radiolabeled it does not show binding in rodent brain.[26,27] Radiosynthesis of [^{18}F]fluoro and [^{11}C]analogues of 2-methoxyestradiol (an

active in vivo metabolite of estrogen), a weak MT ligand, hypoxia inducible factor 1 (HIF-1), and G-protein coupled estrogen receptor (GPER) agonist and [^{18}F] derivative of chelidonine, another weak MT ligand, have also been reported.[28–30] However, no in vivo data are reported for these potential radiotracers. In summary, hitherto there is no successful PET radiotracer available for imaging MTs in brain. Our screen of MT ligands identified MPC-6827 as a candidate ligand. MPC-6827 (verubulin aka Azixa, IC_{50} = 1.5 nM to MT) was selected based on its high MT affinity, selectivity, optimal pharmacokinetics, pharmacodynamics, and in vivo preclinical and clinical information available from literature.[31–36] Furthermore, formation of the *O*-demethylated compound MPI-0440627 (**4**) is likely the major metabolic pathway for MPC-6827 in rodents and human subjects.[34–36] Therefore, radiolabeling of the methoxy group resulting in [^{11}C]MPC-6827, via radiomethylation of MPI-0440627 (desmethyl-MPC-6827) is the most suitable strategy because of the possibility of nonradioactive metabolite formation. This may be an advantage of [^{11}C]MPC-6827 for in vivo applications due to the absence of other competing radioactive metabolites via *O*-demethylation pathway. Herein, we describe the radiosynthesis and in vivo evaluation of *O*-[^{11}C]MPC-6827 aka [^{11}C]MPC-6827 in rodents.

RESULTS

Synthesis of MPC-6827 (**3**) was accomplished via modifications of a previously reported method.[37] Binding affinity and cross selectivity of MPC-6827 to a large panel of brain targets was assessed through NIMH-PDSP. Except for histamine-4 receptor (H_4R, K_i = 155 nM) and sigma-1 receptor (σ_1R, K_i = 426 nM), MPC-6827 did not show significant affinity (K_i = >10000 μM) for all other tested biogenic brain receptors, transporters, enzymes, and protein targets (Table 1). Both H_4R and σ_1 are in comparatively low abundance relative to MTs and therefore are unlikely to interfere with the PET imaging MT quantification by [^{11}C]MPC-6827.

Desmethyl-MPC-6827 (**4**) was synthesized by O-demethy-lation of MPC-6827 with BBr_3 in 85% yield (Scheme 1). The desmethyl product **4**, synthesized via demethylation of the parent molecule, usually contains a very small amount of MPC-6827 (<1%, not detectable by NMR but visible by HPLC) and therefore may interfere with the estimation of specific activity of [^{11}C]MPC-6827. To avoid this situation, we synthesized the radiolabeling precursor **4** via an alternate route by coupling compound **1** with 4-(methylamino)phenol (**5**) in 80% yield (Scheme 1). Radiosynthesis of [^{11}C]MPC-6827 was performed and validated in a GE-FX2MeI/FX2M module by reacting precursor **4** with [^{11}C]CH_3I in the presence of sodium hydroxide as base (Scheme 1). [^{11}C]MPC-6827 was produced with a radiochemical yield (RCY) of 40 ± 5% (n = 20) in >99% radiochemical purity and a specific activity of 2 ± 0.5 Ci/μmol (corrected to end of synthesis (EOS)) in 100% success rate. [^{11}C]MPC-6827 was stable in 5% ethanol–saline formulation under sterile conditions for 4 h (n = 4), and the log $P_{oct/water}$ was estimated as 3.8 by shake flask method (n = 4).

After reliably successful radiosyntheses and stability measurements, we examined the in vivo binding of [^{11}C]MPC-6827 in white male mice by ex vivo biodistribution experiments at 5, 15, 30, and 60 min after tracer tail vein administration in triplicate. [^{11}C]MPC-6827 penetrated the BBB and was retained in the brain (Figure 1A).

The time course of [^{11}C]MPC-6827 in brain indicated a peak at 5 min followed by a gradual washout (Figure 1A). We elected to perform blocking experiments at 30 min based on time—activity curves of [^{11}C]MPC-6827 in baseline experiments (Figure 1A). At 30 min of the biodistribution experiments, 70% specific binding is observed in brain after the administration of MPC-6827 (5 mg/kg, iv) 20 min prior to the radioligand administration (n = 3, Figure 1B). Apart from the brain, muscles, spleen, and lungs showed 60%, 42%, and 30% specific binding, respectively. Pancreas and heart show 20% and 16% specific binding, and no significant specific binding was found in the rest of the tested regions. Therefore, binding in liver and kidney may be attributed to nonspecific binding of [^{11}C]MPC-6827 or its metabolites.

Next, we examined the in vivo binding of [^{11}C]MPC-6827 in athymic nude male mice (n = 3) using microPET. As evident from microPET images (Figure 2), [^{11}C]MPC-6827 penetrates the BBB and shows excellent retention in mouse brain. Brain activity was substantially blocked by the iv administration of 5 mg/kg unlabeled MPC-6827, indicating specific binding of [^{11}C]MPC-6827 to brain MT (n = 3). Of note, radioligand binding in thyroid or salivary gland is also displaced during the blocking experiments (Figure 2). MicroPET experiments in male Sprague—Dawley rats indicate BBB penetration and excellent retention of [^{11}C]MPC-6827 in brain (n = 2) (Figure 3).

DISCUSSION

MPC-6827 is a high affinity, selective MTA (IC_{50} = 1.5 nM) that demonstrated suppression of tumor growth in a variety of cancer animal models, proven safe to use in human subjects, and underwent multiple clinical trials for treatment of glioblastoma (GBM) and a variety of advanced cancers.[31–36] MPC-6827 is proven to be safe in over 100 cancer patients including GBM.[34–36] Although clinical outcome suggests that the drug as a single agent or combination may have limited success in cancer therapy, the BBB penetration, lack of MDR resistance, selective on-target specific binding, facile labeling site, and lack of possible radioactive metabolite and safe use in human subjects are the merits of [^{11}C]MPC-6827 as a potential CNS PET imaging agent for the MT target. Reliability of the automated radiosynthesis of [^{11}C]MPC-6827 was demonstrated by a 100% success rate. Synthesis of MPC-6827 and desmethyl-6827 were accomplished in one step from commercially available precursor chemicals in good yield. The radioligand exhibited BBB penetration in mice and rats and was retained in brain consistent with higher affinity specific binding. The brain uptake of [^{11}C]MPC-6827 was blocked with cold ligand MPC-6827, confirming specific binding. Abundant specific binding of [^{11}C]MP-6827 was also observed in muscle, however, the ratio of specific to nonspecific binding in brain is 10 times higher than in muscle (Figure 1B). [^{11}C]MPC-6827 activity in brain was peaked at 5 min, followed by a gradual washout indicating favorable kinetics for tracer quantification in mouse brain (Figure 1A). We did not find blockade of radioligand binding in the heart. In blood, there is high plasma binding (98.2%) of the parent ligand in rodents.[36] Kidney and liver show high accumulation of activity in mice, and the binding was not displaced with cold MPC-6827 in blocking experiments. This uptake may be related to metabolism and excretion of the tracer and its metabolites. Therefore, [^{11}C]MPC-6827 may not be a good PET radiotracer for imaging tumors in lower thorax or abdomen in mice. To the best of our knowledge, [^{11}C]MPC-6827

is the first MT radioligand that penetrates the BBB and specific binding in vivo in rodents. [^{11}C]MPC-6827 may be a viable radiotracer for the in vivo imaging of normal MT functions and animal models with altered brain functions with MT pathology due to its specific binding and favorable kinetics.

CONCLUSIONS

In summary, we developed an automated synthesis of [^{11}C]MPC-6827, a high affinity and selective MT ligand, in high yield, purity, and specific activity. In vivo studies in rodents indicated BBB penetration and binding of the radiotracer in brain and other organs or tissues. Specificity of [^{11}C]MPC-6827 binding was demonstrated by blocking studies with cold ligand MPC-6827. Combination of rapid washout and robust specific binding with excellent brain uptake may make [^{11}C]MPC-6827 a suitable PET ligand for the in vivo quantification of MT inside and outside of the brain.

EXPERIMENTAL SECTION

General Considerations.

Solvents are of reagent grade or higher purity. All reagents were purchased from commercial vendors in >95% purity and used as received. ^{l}H NMR spectra were recorded on a Bruker PPX 400-MHz spectrometer. Spectra were recorded in CD_3OD, and chemical shifts (δ) are reported in parts per million (ppm) relative to tetramethylsilane. The mass spectra were recorded on a JKS-HX 11UHF/HX110 HF tandem mass spectrometer in the fast atom bombardment (EI+) mode. Thin-layer chromatography was performed using silica gel 60 F254 plates from E. Merck (Aston, PA). High-performance liquid chromatography (HPLC) analyses were performed using a Waters 1525 HPLC system (Milford, MA), and flash column chromatography was performed on silica gel (Fisher 200–400 mesh) using the solvent system indicated in the experimental procedure for each compound. Chemical purities of biologically tested compounds MPC-6827 and desmethyl-MPC-6827 were >95% based on reverse phase HPLC (RP-HPC) analyses using UV detector at 254 nM. The purities (chemical and radiochemical) and stability of [^{11}C]MPC-6827 were determined by RP-HPLC (Torrance, CA) with photodiode array and sodium iodide detectors. Lipophilicity (expressed as log $P_{oct/water}$) of [“C]MPC-6827 was estimated by determining the partition coefficient between 1-octanol and freshly prepared phosphate buffer using a standard shake flask method as described elsewhere.[38] Biodistribution studies were performed in male white mice, and radioactivity counts were measured using a Wallac 1480 Wizard gamma counter, PerkinElmer, Turku, Finland.[39] microPET studies were performed in Sprague—Dawley rats and athymic male nude mice Trifoil PET/CT scanner under anesthetic condition.[40] All animal experiments were carried out with the approval of the Institutional Animal Care and Use Committee of Wake Forest University Medical Center.

Desmethyl-MPC-6827 (4).

First, 2 mL of anhydrous dichloromethane (DCM) was added to an argon charged reaction vessel containing MPC-6827 (85 mg, 0.3 mmol) at 0 °C. Then 1 M solution of BBr3 in DCM (1 mL) was added dropwise to it at 0 °C. The solution was stirred for 1 h at room

temperature. An aliquot of reaction mixture was quenched with methanol, analytical HPLC performed, and complete conversion of MPC-6827 conformed. The reaction was quenched by dropwise addition of methanol (1 mL) at 0 °C, diluted with water (5 mL), extracted with 50 mL of DCM (2 × 25 mL), followed by 50 mL of ethyl acetate (2 × 25 mL). The combined organic extracts were washed with brine and dried over anhydrous $MgSO_4$. Solvent was evaporated under reduced pressure, and the residue obtained was washed with ice-cold hexane to obtain compound **4** (70 mg, 85%) as a yellow solid. **4**: ^{1}H NMR (400 MHz, CD_3OD) δ: 2.7 (s, 3H), 3.7 (s, 3H), 6.8 (m, 3H), 7.1 (m, 3H), 7.6 (m, 2H). HRMS (EI +): calculated for $C_{16}H_{16}N_3O$ 266.1293, found 266.1294.

Alternative Synthesis of Compound 4.

To a solution of 4-chloro-2-methylquinazoline (**1**, 90 mg, 0.5 mmol) and 4-(methylamino)-phenol (**5**, 70 mg, 5.75 mmol) in 2 mL of anhydrous 2-propanol (IPA) added 2 drops of concentrated HCl, and the reaction mixture was stirred at room temperature overnight. The yellow precipitate was collected by filtration, washed with cold 2-propanol, and dried under vacuum to afford compound **4** (105 mg, 80%) as a yellow solid. Analytical data of compound **4** is identical with the product obtained using previous method.

Radiosynthesis of [^{11}C]MPC-6827.

[^{11}C]MeI from FX2MeI module was bubbled to the reaction vial placed in FX2M module containing precursor **4** (~0.5—0.8 mg) in anhydrous DMF (0.6 mL) and 5 N NaOH aqueous solution (10.0 μL) for ~5 min at room temperature. After the complete transfer of radioactivity, the sealed reaction vial was then heated at 80 °C for 5 min. The reaction mixture was quenched with HPLC mobile phase (1.0 mL) and injected onto a reverse-phase semipreparative C18 Phenomenex ODS (250 mm × 10 mm, 10 μ) HPLC column to purify [^{11}C]MPC-6827. The isocratic HPLC mobile phase solution consisted of 60% acetonitrile, 40% 0.1 M aqueous ammonium formate buffer solution (pH 6.0—6.5) with UV λ @ 254 nm and a flow rate of 7.0 mL/min. The product [^{11}C]MPC-6827 (R_t = 9.0—11.0 min) was collected and diluted with 100 mL of deionized water and passed through C18 SepPak cartridge (WAT036800, Waters, Milford, MA) to trap the radioactive product. [^{11}C]MPC-6827 was then directly eluted from the cartridge with absolute ethanol (1.0 mL) and formulated with saline (10% ethanol in saline) into a sterile vial through a sterile 0.22 μm pyrogen-free filter for further animal studies and quality control analysis. [^{11}C]MPC-6827 purity was assessed using an analytical Phenomenex C18 HPLC column (250 mm × 4.6 mm, 5 μ) and with UV λ @ 254 nm. The mobile phase (1.0 mL/min) consisted of 60% acetonitrile and 40% 0.1 M aqueous ammonium formate pH 6.0—6.5 solution. [^{11}C]MPC-6827 showed a retention at 7.1 min, and authentication of the product was performed with coinjection of the nonradioactive standard MPC-6827, which demonstrated a similar retention times.

Biodistribution of [^{11}C]MPC-6827 in Mice.

Biodistribution experiments were performed as described previously.[39] Briefly, 100 ± 20 μCi of [^{11}C]MPC-6827 were administered to male white mice in 10% ethanol—saline (100 μL per 100 g body weight) through tail vein injection without anesthesia. Uptake of radiotracer

in different organs such as brain, heart, lungs, liver, kidney, spleen, pancreas, muscles, and blood were calculated as percentages of injected dose per gram of tissue (%ID/g tissue). Tracer uptakes in the tissues were measured using a γ-counter and expressed in %ID/g tissue. Specific binding were demonstrated by performing blocking studies of cold-ligand MPC- 6827 (5 mg/kg, iv) 20 min prior to radiotracer administration, and dissections were performed at 30 min post radiotracer injection. All experiments were performed in triplicate.

microPET Imaging of [^{11}C]MPC-6827 in Mice and Rats.

microPET imaging of [^{11}C]MPC-6827 was performed as described previously.[40] In brief, microPET experiments were performed in anesthetized white male mice (n = 3) or Sprague-Dawey rats (n = 2) using Trifoil PET/CT scanner. After the transmission scans, [^{11}C]MPC-6827 (50 ± 10 μCi for mice and 100 ± 20 μCi for rats) was injected into the tail vein and initiated camera acquisition for 60 min and reconstructed using attenuation correction and Fourier rebinning. Blocking microPET imaging were performed in white male mice (n = 3) 20 prior to the injection of MPC-6827 (5 mg/kg, iv). The dynamic images were reconstructed using a filtered back-projection algorithm (microPET Manager).

Supplementary Material

Refer to Web version on PubMed Central for supplementary material.

ACKNOWLEDGMENTS

We thank NIMH-PDSP for competitive binding assay of MPC-6827. This work was supported by Diane Goldberg Foundation (CUMC/NYSPI) and Translational Imaging Program (TIP) of the Wake Forest CTSA (UL1TR001420).

ABBREVIATIONS USED

AD	Alzheimer’s Disease
ALS	amyotrophic lateral sclerosis
BBB	blood—brain barrier
BCRP	breast cancer resistance protein
CTE	chronic traumatic encephalopathy
CNS	central nervous system
CBD	corticobasal degeneration
EOS	end of synthesis
GBM	glioblastoma multiform
GPER	G-protein coupled estrogen receptor
HSP	hereditary spastic paraplegia
H4R	histamine-4 receptor

HD	Huntington's disease
HIF-1	hypoxia inducible factor 1
MT	microtubule
MTA	microtubule targeting agent
MDR1	multidrug resistance protein 1
MS	multiple sclerosis
PD	Parkinson's disease
P-gp	permeability glycoprotein
PET	positron emission tomography
PSP	progressive supranuclear palsy
RCY	radiochemical yield
σ1R	sigma 1 receptor
SCI	spinal cord injury
TBI	traumatic brain injury

REFERENCES

(1). Janke C The tubulin code: molecular components, readout mechanisms, and functions. J. Cell Biol. 2014, 206 (4), 461–472. [PubMed: 25135932]

(2). Nogales E Structural insights into microtubule function. Annu. Rev. Biochem. 2000, 69, 277–302. [PubMed: 10966460]

(3). Hur EM; Lee BD Microtubule-targeting agents enter the central nervous system (CNS): double-edged swords for treating CNS injury and disease. Int. Neurourol J. 2014, 18 (4), 171–178. [PubMed: 25558415]

(4). Eira J; Silva CS; Sousa MM; Liz MA The cytoskeleton as a novel therapeutic target for old neurodegenerative disorders. Prog. Neurobiol. 2016, 141, 61–82. [PubMed: 27095262]

(5). Brunden KR; Lee VM; Smith AB 3rd; Trojanowski JQ; Ballatore C Altered microtubule dynamics in neurodegenerative disease: Therapeutic potential of microtubule-stabilizing drugs. Neurobiol. Dis. 2017, 105, 328–335. [PubMed: 28012891]

(6). Florian S; Mitchison TJ Anti-microtubule drugs. Methods Mol. Biol. 2016, 1413, 403–421. [PubMed: 27193863]

(7). Wilson L; Jordan MA New microtubule/tubulin-targeted anticancer drugs and novel chemotherapeutic strategies. J. Chemother. 2004, 16 (4), 83–85.

(8). Dostál V; Libusová L Microtubule drugs: action, selectivity, and resistance across the kingdoms of life. Protoplasma 2014, 251 (5), 991–1005. [PubMed: 24652407]

(9). Mitchell D; Bergendahl G; Ferguson W; Roberts W; Higgins T; Ashikaga T; DeSarno M; Kaplan J; Kraveka J; Eslin D; Werff AV; Hanna GK; Sholler GL A Phase 1 trial of TPI 287 as a single agent and in combination with Temozolomide in patients with refractory or recurrent neuroblastoma or medulloblastoma. Pediatr. Blood Cancer 2016, 63 (1), 39–46. [PubMed: 26235333]

(10). Penazzi L; Bakota L; Brandt R Microtubule dynamics in neuronal development, plasticity, and neurodegeneration. Int. Rev. Cell Mol. Biol. 2016, 321, 89–169.

(11). Kovalevich J; Cornec AS; Yao Y; James M; Crowe A; Lee VM; Trojanowski JQ; Smith AB 3rd; Ballatore C; Brunden KR Characterization of brain-penetrant pyrimidine-containing molecules with differential microtubule-stabilizing activities dveloped as potential therapeutic agents for Alzheimer's Disease and related tauopathies. J. Pharmacol. Exp. Ther. 2016, 357 (2), 432–450. [PubMed: 26980057]

(12). Dent EW Of microtubules and memory: implications for microtubule dynamics in dendrites and spines. Mol. Biol. Cell 2017, 28 (1), 1–8. [PubMed: 28035040]

(13). Cappelletti G; Casagrande F; Calogero A; De Gregorio C; Pezzoli G; Cartelli D Linking microtubules to Parkinson's disease: the case of parkin. Biochem. Soc. Trans. 2015, 43 (2), 292–296. [PubMed: 25849932]

(14). Clark JA; Yeaman EJ; Blizzard CA; Chuckowree JA; Dickson TC A case for microtubule vulnerability in Amyotrophic Lateral Sclerosis: altered dynamics during disease. Front. Cell. Neurosci. 2016, 10, 204. [PubMed: 27679561]

(15). Zempel H; Mandelkow EM Tau missorting and spastin-induced microtubule disruption in neurodegeneration: Alzheimer Disease and Hereditary Spastic Paraplegia. Mol. Neurodegener. 2015, 10, 68. [PubMed: 26691836]

(16). Mastronardi FG; Moscarello MA Molecules affecting myelin stability: a novel hypothesis regarding the pathogenesis of multiple sclerosis. J. Neurosci. Res. 2005, 80 (3), 301–308. [PubMed: 15704220]

(17). Fernández-Nogales M; Santos-Galindo M; Hernández IH; Cabrera JR; Lucas JJ Faulty splicing and cytoskeleton abnormalities in Huntington's disease. Brain Pathol. 2016, 26 (6), 772–778. [PubMed: 27529534]

(18). Paula-Barbosa M; Tavares MA; Cadete-Leite A A quantitative study of frontal cortex dendritic microtubules in patients with Alzheimer disease. Brain Res. 1987, 417, 139–142. [PubMed: 3620973]

(19). Yan SB; Hwang S; Rustan TD; Frey WH Human brain tubulin purification: decrease in soluble tubulin with age. Neurochem. Res. 1985, 10, 1–18. [PubMed: 3982586]

(20). Katsetos CD; Dráber P Tubulins as therapeutic targets in cancer: from bench to bedside. Curr. Pharm. Des. 2012, 18 (19), 2778–2792. [PubMed: 22390762]

(21). Laggner U; Pipp I; Budka H; Hainfellner JA; Preusser M Immunohistochemical detection of class III beta-tubulin in primary brain tumours: variable expression in most tumour types limits utility as a differential diagnostic marker. Histopathology 2007, 50 (7), 949–952. [PubMed: 17543088]

(22). Katsetos CD; Dráberová E; Legido A; Dumontet C; Dráber P Tubulin targets in the pathobiology and therapy of glioblastoma multiforme. I. Class III beta-tubulin. J. Cell. Physiol. 2009, 221 (3), 505–513. [PubMed: 19650075]

(23). van der Veldt AA; Lammertsma AA In vivo imaging as a pharmacodynamic marker. Clin. Cancer Res. 2014, 20 (10), 2569–2577. [PubMed: 24831279]

(24). Yang CH; Horwitz SB Taxol®: The first microtubule stabilizing agent. Int. J. Mol. Sci 2017, 18 (8), 1733–1744.

(25). Banerjee S; Hwang DJ; Li W; Miller DD Current advances of tubulin inhibitors in nanoparticle drug delivery and vascular disruption/angiogenesis. Molecules 2016, 21 (11), 1468–1487.

(26). Hendrikse NH; Franssen EJ; van der Graaf WT; Vaalburg W; de Vries EG Visualization of multidrug resistance in vivo. Eur. J. Nucl. Med. Mol. Imaging 1999, 26 (3), 283–293.

(27). Levchenko A; Mehta BM; Lee JB; Humm JL; Augensen F; Squire O; Kothari PJ; Finn RD; Leonard EF; Larson SM Evaluation of 11C-colchicine for PET imaging of multiple drug resistance. J. Nucl. Med. 2000, 41 (3), 493–501. [PubMed: 10716325]

(28). Mun J; Voll RJ; Goodman MM Synthesis of 2-[11C]methoxy-3,17β-estradiol to measure the pharmacokinetics of an antitumor drug candidate, 2-methoxy-3,17β-estradiol. J. Labelled Compd. Radiopharm. 2006, 49, 1117–1124.

(29). Mun J; Wang Y; Voll RJ; Escuin-Borras D; Giannakakou P; Goodman MM Syntheses and biological activities of novel 2-methoxyestradiol analogs, 2-fluoroethoxyestradiol and 2-fluoropropa-noxyestradiol, and a radiosynthesis of 2-[(18)F]fluoroethoxyestradiol for positron emission tomography. Nucl. Med. Biol. 2008, 35 (5), 615–622. [PubMed: 18589306]

(30). Jalilian AR; Seyfi P; Afarideh H; Shafiee A Synthesis of a [18F]labeled chelidonine derivative as a possible antitumor agent. Appl Radiat. Isot. 2001, 54 (3), 407–411. [PubMed: 11214874]

(31). Kasibhatla S; Baichwal V; Cai SX; Roth B; Skvortsova I; Skvortsov S; Lukas P; English NM; Sirisoma N; Drewe J; Pervin A; Tseng B; Carlson RO; Pleiman CM MPC-6827: a small-molecule inhibitor of microtubule formation that is not a substrate for multidrug resistance pumps. Cancer Res. 2007, 67 (12), 5865–5871. [PubMed: 17575155]

(32). Sirisoma N; Pervin A; Zhang H; Jiang S; Willardsen JA; Anderson MB; Mather G; Pleiman CM; Kasibhatla S; Tseng B; Drewe J; Cai SX Discovery of N-(4-methoxyphenyl)-N,2-dimethylquinazolin-4-amine, a potent apoptosis inducer and efficacious anticancer agent with high blood brain barrier penetration. J. Med. Chem. 2009, 52 (8), 2341–2351. [PubMed: 19296653]

(33). Mahal K; Resch M; Ficner R; Schobert R; Biersack B; Mueller T Effects of the tumor-vasculature-disrupting agent verubulin and two heteroaryl analogues on cancer cells, endothelial cells, and blood vessels. ChemMedChem 2014, 9 (4), 847–854. [PubMed: 24678059]

(34). Chamberlain MC; Grimm S; Phuphanich S; Recht L; Zhu JZ; Kim L; Rosenfeld S; Fadul CE Brain tumor investigational consortium. A phase 2 trial of verubulin for recurrent glioblastoma: a prospective study by the Brain Tumor Investigational Consortium (BTIC). J. Neuro-Oncol. 2014, 118 (2), 335–343.

(35). Grossmann KF; Colman H; Akerley WA; Glantz M; Matsuoko Y; Beelen AP; Yu M; De Groot JF; Aiken RD; Olsen JJ; Evans BA; Jensen RL Phase I trial of verubulin (MPC-6827) plus carboplatin in patients with relapsed glioblastoma multiforme. J. Neuro-Oncol. 2012, 110 (2), 257–264.

(36). Tsimberidou AM; Akerley W; Schabel MC; Hong DS; Uehara C; Chhabra A; Warren T; Mather GG; Evans BA; Woodland DP; Swabb EA; Kurzrock R Phase I clinical trial of MPC-6827 (Azixa), a microtubule destabilizing agent, in patients with advanced cancer. Mol. Cancer Ther. 2010, 9 (12), 3410–3419. [PubMed: 21159616]

(37). Lockman JW; Klimova Y; Anderson MB; Willardsen JA Synthesis of substituted quinazolines: Application to the synthesis of verubulin. Synth. Commun. 2012, 42 (12), 1715–1723.

(38). Wilson AA; Jin L; Garcia A; DaSilva JN; Houle S An admonition when measuring the lipophilicity of radiotracers using counting techniques. Appl. Radiat. Isot. 2001, 54 (2), 203–208. [PubMed: 11200881]

(39). Solingapuram Sai KK; Das BC; Sattiraju A; Almaguel FG; Craft S; Mintz A Radiolabeling and initial biological evaluation of [18F]KBM-1 for imaging RAR-a receptors in neuroblastoma. Bioorg. Med. Chem. Lett. 2017, 27 (6), 1425–1427. [PubMed: 28216044]

(40). Solingapuram Sai KK; Prabhakaran J; Sattiraju A; Mann JJ; Mintz A; Kumar JSD Radiosynthesis and evaluation of IGF1R PET ligand [11C]GSK1838705A, Bioorg. Bioorg. Med. Chem. Lett. 2017, 27 (13), 2895–2897. [PubMed: 28479199]

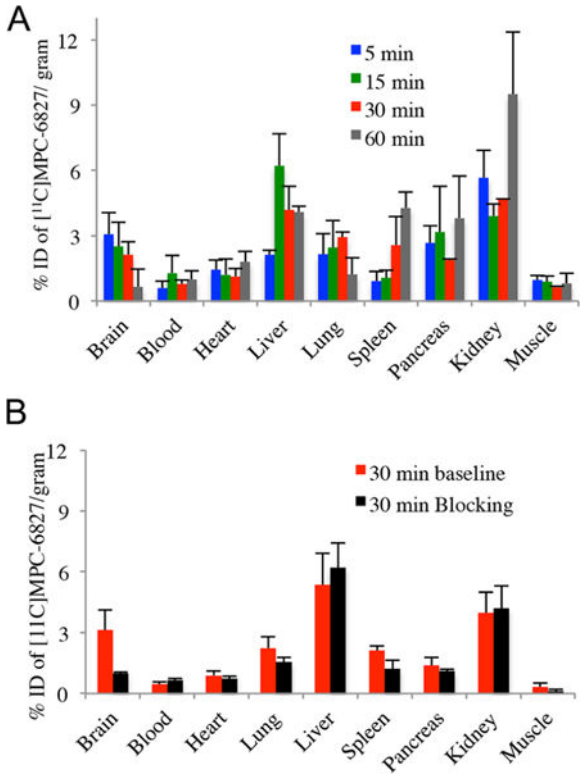

Figure 1.

(A) Baseline biodistribition of [^{11}C]MPC-6827 in male white mice (n = 3). (B) Blocking biodistriution of [^{11}C]MPC-6827 in mice at 30 min (n = 3)

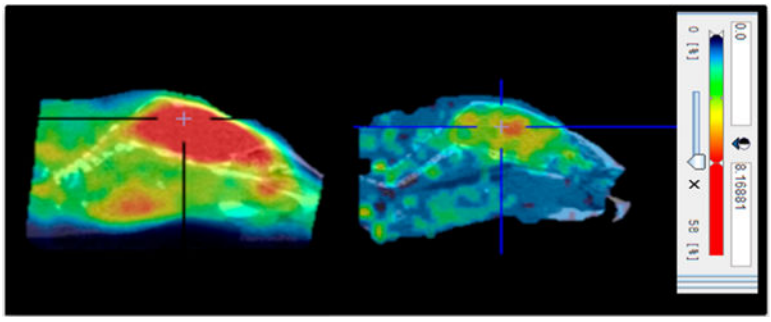

Figure 2.

Sum of 0–60 min microPET sagittal images of [^{11}C]MPC-6827 in a representative mouse brain (left, baseline; right, blocking with 5 mg/kg MPC-6827; cross lines represent center of brain).

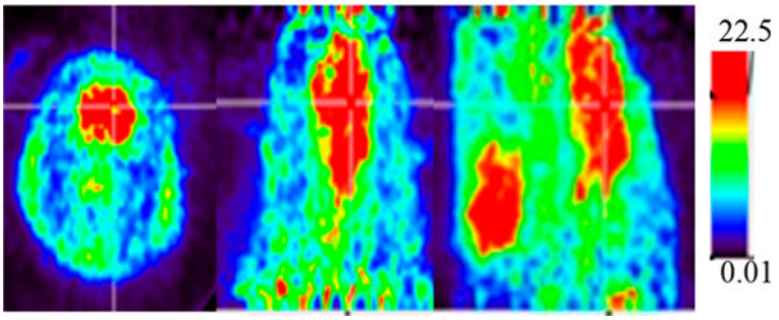

Figure 3.

Sum of 0–60 min microPET sagittal images of [^{11}C]MPC-6827 in rat brain (left, transverse; middle, coronal; right, sagittal; cross lines represent center of brain).

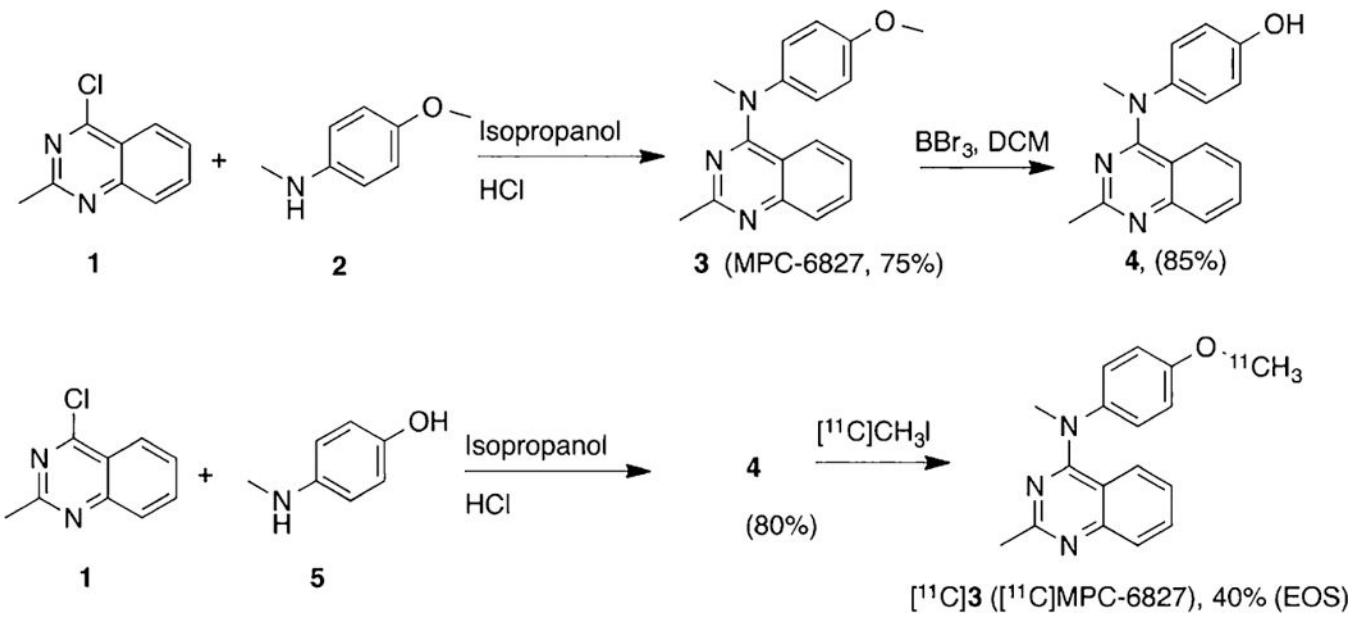

Scheme 1.
Synthesis of MPC-6827 and Radiosynthesis of [^{11}C]MPC-6827

Table 1.

Affinity of MPC-6827 to Brain Targets[a]

targets	affinity (nM)	targets	affinity (nM)
MT	1.5[31,32]	5-HT1A-1E	>10000
5-HT2A-2C	>10000	5-HT3-7	>10000
5-HT2A-2C	>10000	A	>10000
5-HT3–7	>10000	α1A-1C	>10000
α2A-2C	>10000	β1–3	>10000
AMPA	>10000	BZP	>10000
Ca+ channel	>10000	CB1, CB2	>10000
D1-D5	>10000	DAT	>10000
DOR	>10000	H1	>10000
H2	155	H3, H4	>10000
HERG	>10000	GABA	>10000
EP	>10000	I	>10000
KOP	>10000	KA	>10000
M	>10000	mGluR	>10000
MDR1	>10000	MOR	6479
NET	>10000	NK	>10000
NMΔA	>10000	NOP	>10000
NT	>10000	oxytocin	>10000
PBR	>10000	PKC	>10000
SERT	>10000	σ1	426
σ2	>10000	Na + channel	>10000
smoothened	>10000	VMAT 1,2	>10000

[a]MT, microtubule; 5-HT, 5-hydroxytryptamin; A, adenosine; α, alpha; β,: beta; BZP, benzodiazepine; AMPA, *R*-amino-3-hydroxy-5-methyl-4-isoxazolepropionic acid; CB, cannabinoid; D, dopamine; DAT, dopamine transporters; DOR, δ opioid receptors; EP, prostanoid receptors: GABA, γ-amino butyric acid; H, histamine; hERG, human ether-a-go-go; KA, kainate; KOR, κ opioid receptors; M, muscarinic; MDR, multidrug resistance; MOR, μ opioid receptor; mGluR, metabotropic glutamate receptors; NMDA, *N*-methyl-D-aspartic acid; NK, neurokinin; NET, norepinephrine transporter; NT, neurotrophin; PKC, protein kinase C; SERT, serotonin transporter; V, vasopressin; VMAT, vesicular monoamine transporter.